A Strategy for Polar Crystals with Dipolar Heterohelicenes

Satoru Hiroto*, Mana Wakita, Moeko Chujo

Dedication ((optional))

[a]   M. Wakita, Dr. M. Chujo, Prof. Dr. S. Hiroto
        Graduate School of Human and Environmental Studies
        Kyoto University
        Nihonmatsu-cho, Yoshida, Sakyo-ku, Kyoto 606-8501, Japan
        E-mail: hiroto.satoru.4a@kyoto-u.ac.jp
        Supporting information for this article is given via a link at the end of the document.

Abstract: Polar crystals have attracted interest for the applications to polar materials with piezo- and pyroelectricity, and second harmonic generation. Despite their potential utility for flexible polar materials, a strategy for ordering polar helicenes have remained elusive. Here, we demonstrate creation of polar crystal with unsymmetrically substituted aza[5]helicenes tuned by substituents. The unsymmetric aza[5]helicenes have been prepared through regioselective mono-protiodesilylations. We disclosed triisopropylsilyl-substituted derivatives show 1D chain columnar packings. In particular, enantiopure crystals showed spontaneous polarization. Optical and single-crystal X-ray diffraction experiments with other derivatives, as well as theoretical calculations, revealed that the presence of triisopropylsilyl or electron-withdrawing aryl substituents is essential for forming the 1D chain columnar structure. Hirshfeld surface analyses further showed that CH-π interactions between 1D chain columns regulate the polar assembly. Finally, we determined the polarizability of the nitro derivative by *ab initio* calculation to be 4.53 μC/cm^2. This value corroborates the first example of a spontaneously polar crystal of helicenes. We believe that this study will contribute to the development of polar materials from organic molecules.

Introduction

Controlling the assembly of π-conjugated molecules in the solid state is an important factor in the attainment of desired functions and high-performance properties, such as electronic conductivity and non-linear optics, for solid-state organic materials.[1] In particular, the alignment of polar π-conjugated molecules in non-centrosymmetric order is essential for piezo-, pyro-, and ferroelectricity and for the generation of second harmonics.[2] However, polar π-conjugated molecules usually form π-dimers in an anti-parallel manner as a thermodynamically favored conformation because of dipole-dipole interactions.[3] Therefore, intermolecular interactions, such as hydrogen bonding, van der Waals interactions with alkyl chains, and π-π stacking, have usually been adopted to force polar π-conjugated molecules to be ordered in a parallel manner.[4]

Recently, curved π-conjugated molecules, such as buckybowls, helicenes, and carbon nanohoops, have attracted much attention for their potential applications to molecular devices because of their anisotropic structures, which provide anisotropic transporting characteristics in electron or charge distribution for molecular electronic devices.[5,6] Although there have been some studies on the assembly of curved π-conjugated molecules, mainly with bowl-shaped π-conjugated molecules, the

strategies for controlling their assembly in the crystal state remain challenging.[7,8] One reason for the difficulty in assembly is that their anisotropic structures are incompatible with regularity in packing. The second reason is the difficulty in their accessibility due to their strained structures, which have limited straightforward design for controlling their alignments in the solid state.[9,10] Under such conditions, the construction of a polar crystal with curved π-conjugated molecules is a major focus of research in organic chemistry.

In this study, we focus on helicenes, which are helical π-conjugated molecules.[11] Recent development of helicene chemistry has been emerging because of the unique properties of their helical and rigid structures, which cause these molecules to exhibit structurally related chiroptical properties and catalytic activity.[12] Helicenes have two enantiomers, the (*P*)-helix and the (*M*)-helix. We thought that their asymmetric features would facilitate alignment in a non-centrosymmetric order to form polar crystals. In addition, helicenes have recently been reported as promising candidates for organic piezoelectric materials.[13] In 2018, Starý and co-workers reported the large converse piezoelectric response of functionalized helicenes on metal surfaces.[14] Thus, assembling helicenes in a polar manner should be important to developing their potential to function as organic piezoelectric materials. There have been several reports on ordering the crystal packing of helicenes by using weak intermolecular interactions such as hydrogen bonding and π-π stackings.[15] Although some researchers have reported the synthesis of unsymmetrical helicenes by inclusion of heteroatoms or electron-withdrawing substituents, a polar assembly of helicenes has not been achieved or asserted, to our knowledge.[16] In a study of bowl-shaped π-conjugated molecules, Miyajima *et al.* recently demonstrated a strategy for the formation of polar crystals with subphthalocyanines.[17] They reported a clever installation of fluorine substituents at the periphery to form CF-H intermolecular interactions, which regulated the assembly of columns. For helicenes, an alternative strategy for the formation of a polar 1D chain columnar structure should be required, in contrast to bowl-shaped π-conjugated molecules, for which a bowl-to-bowl packing by concave-convex interactions facilitates the formation of a polar column.
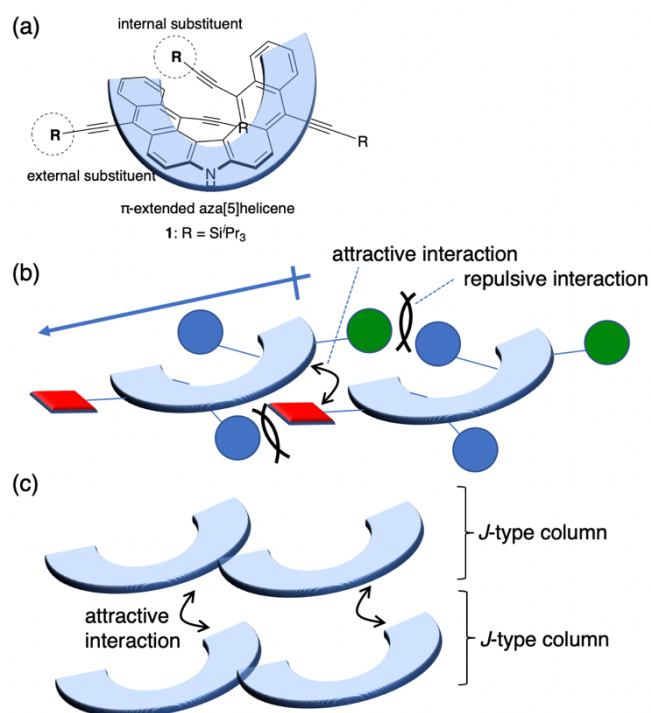
Chart 1. (a) π-extended azahelicene **1** and (b) the slip-stacked strategy for *J*-type columnar assembly.

Herein, we investigate the substituent effect of π-extended aza[5]helicenes on the assembly in a crystal.[18] The π-extended aza[5]helicenes can bear alkynyl substituents at both external and internal positions of the helix. In the previous study, we succeeded in the regioselective protiodesilylation of the π-extended aza[5]helicene **1** with Bu₄NF under controlled conditions.[19] We thought that by using this method, we could explore the conditions of substituents that could control the sequence between columns. A *J*-type columnar assembly would be achieved by the introduction of attractive interactions, such as π-π stacking between the outer substituent of one molecule and the azahelicene core of another molecule, and repulsive interactions, such as steric repulsion between the internal substituent of one molecule and the external substituent of the other (Chart 1). Such *J*-type assembly enable to form vertical stacking due to its availability for another intermolecular interactions. Consequently, we succeeded in the construction of polar crystals with dipolar and unsymmetrically substituted aza[5]helicenes.

Results and Discussion

As reported previously,[18a] the treatment of π-extended aza[5]helicene **1** with Bu₄NF at 0 °C provided double-protiodesilylated product **2b** with high regioselectivity (entry 1). In this study, we isolated a non-negligible amount of mono-protiodesilylated product **2a**. We optimized the reaction conditions to obtain **2a** in higher yield. Afterwards, we disclosed that CsF as a fluoride source proved effective. In THF, no reaction proceeded in the presence of 1.0 equiv. of CsF at room temperature (entry 2), whereas the protiodesilylation proceeded in DMF, providing **2a** in 38% yield (entry 3). Finally, 2.5 equiv. of CsF improved the yield

of **2a** up to 59% (entry 4). Other fluoride source such as AgF, reported effective for desilylation, did not work well (entry 5).[20] The structure of **2a** was determined by NMR spectroscopy and X-ray diffraction analysis. Its ¹H NMR spectrum exhibited one singlet proton at 4.05 ppm due to a terminal alkyne. In addition, the remaining signals around 0 ppm because of the internal triisopropylsilyl (TIPS) substituents indicated that the reaction occurred at the external position. Finally, we determined the structure by single-crystal X-ray diffraction analysis. As shown in Figure 1a, one silyl group of **1** was substituted with a proton with high regioselectivity.
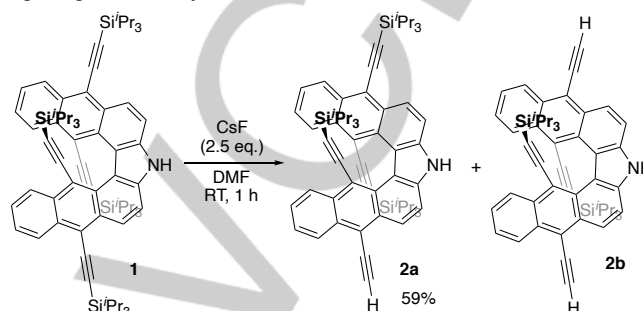

Entry	Fluoride source (equiv.)	Solvent	Temp. (°C)	Time	Yields (%)	
					2a	**2b**
1	Bu₄NF (2.0)	THF	0	20 min	0	89
2	CsF (1.5)	THF	RT	1 h	0	0
3	CsF (1.0)	DMF	RT	3 h	38	trace
4	CsF (2.5)	DMF	RT	1 h	59	N.D.ᵃ
5	AgF (1.5)	DMF	RT	8 h	0	0

a: Not determined

Scheme 1. Regioselective protiodesilylation of **1** to **2a** and **2b**.

With the mono-protiodesilylated product **2a** in hand, we set out to introduce aryl substituents (Scheme 2). First, we introduced a 3,5-di-*tert*-butylphenyl substituent through a Sonogashira-Hagihara cross-coupling reaction with 3,5-di-*tert*-butyl-1-iodobenzene, furnishing the product **3a** in 80% yield. Following a similar procedure to that followed to produce **3a**, we prepared 4-cyanophenyl- (**3b**), 4-nitrophenyl- (**3c**), 4-pyridyl- (**3d**), phenyl- (**3e**), and mesityl- (**3f**) substituted derivatives in appreciable yields. Further treatment of **3a** with Bu₄NF at –10 °C, followed by protonation with aqueous HCl, provided the mono-protiodesilylated product **4a** in 97% yield; the reaction occurred exclusively at the external silyl substituent. Eventually, we obtained aza[5]helicenes with different aryl substituents—**5a** and **5b**—by Sonogashira-Hagihara cross-coupling of **4a** with 4-iodobenzonitrile and 1-iodo-4-nitrobenzene in 70% and 94% yield, respectively. Following the same procedure, we also performed the protiodesilylation of **3f**, followed by installation of a 4-cyanophenyl substituent to obtain **5c**. We also succeeded in the preparation of the enantiomerically pure products (***M***)-**3b** and (***M***)-**3c** from (***M***)-**1**, according to the same procedure that was followed for their racemic counterparts.
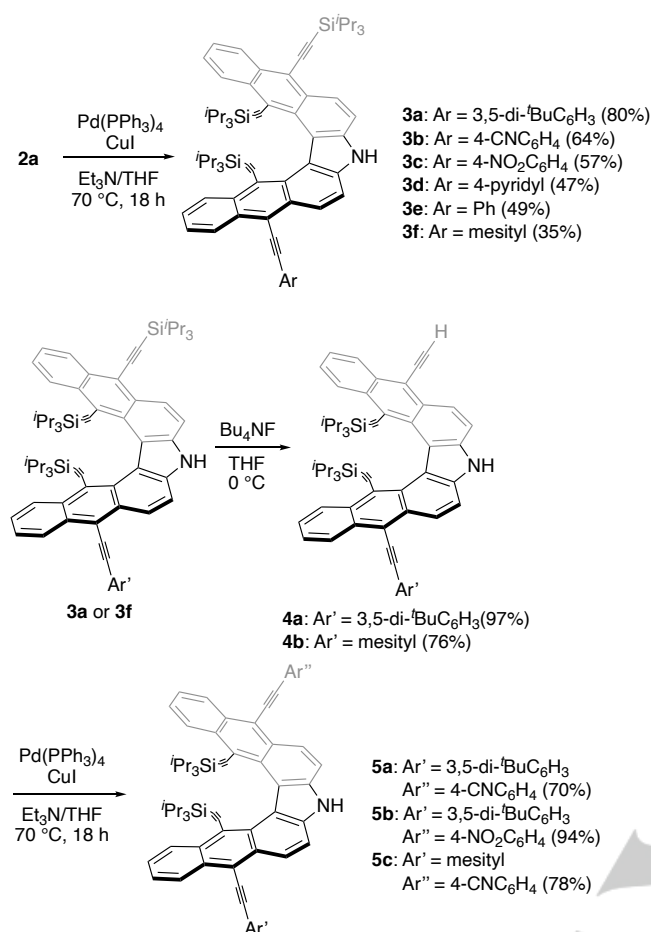
Scheme 2. Synthesis of asymmetrically substituted aza[5]helicenes using regioselective desilylation and the Sonogashira coupling reaction.

Figure 1. X-ray crystal structures of **2a**, (**M**)-**3b**, and **5a**. (a) Top view and (b) front view of **2a**, (c) top view and (e) front view of (**M**)-**3b**, and (d) top view and (f) front view of **5a**. The hydrogen atoms are omitted for clarity, except for those in **(a)**. The thermal ellipsoids are scaled at the 50% probability level.

The characterizations of all products were performed by NMR and mass spectroscopic analysis. Furthermore, the solid-state structures of **2a**, (**M**)-**3b**, **3c**, (**M**)-**3c**, **3d**, **3e**, **5a**, and **5c** were elucidated by single-crystal X-ray diffraction analysis.[21] Figure 1c, d, and e and Figure 1f display the crystal structures of the cyano-substituted derivatives (**M**)-**3b** and **5a**, respectively. In (**M**)-**3b**, the aryl group exhibited almost perfect co-planarity to the covalently bound azahelicene unit, in which the dihedral angle between the two mean planes was 23.8°, which is within the expected range for the presence of a π-electronic interaction (Table S2). Similar coplanarity of the 4-cyanophenyl substituent was observed for compound **5a** with a dihedral angle of 6.55°. However, the 3,5-di-*tert*-butylphenyl substituent of **5a** was tilted towards the azahelicene core. The tilting angle of the aryl group from the mean plane between the three carbon atoms C(4), C(5), and C(6) was 71.2°. The mesityl group of **5c** showed almost perfectly coplanar geometry (Figure S29), indicating that intermolecular interactions with neighboring molecules may induce the displacement. The difference in the tilting angles indicate that the electronic interactions with azahelicene cores for these aryl-substituted derivatives are varied.
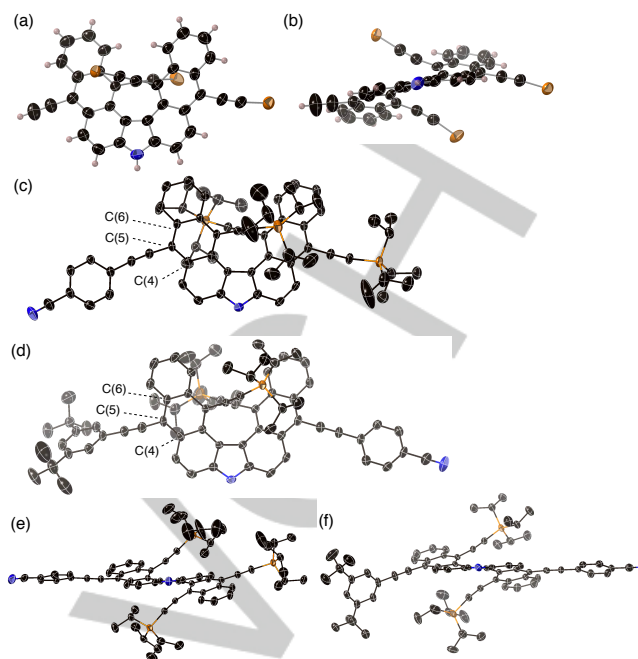
The unsymmetrically substituted aza[5]helicenes should have dipole moments, owing to the presence of intermolecular charge transfer (ICT) characteristics. To verify the ICT characteristics of these molecules, we investigated the effect of the solvent on the optical properties. Figure 2a describes the UV/vis absorption spectra of **2a**, **3a**, **3b**, **3c**, **3d**, and **3e** in toluene. Compared with **2a**, each aza[5]helicene with an electron-withdrawing group exhibits an additional broad band as its lowest-energy transition. To assign this band, we performed theoretical calculations. The structure of **3b** was further optimized based on the density functional theory (DFT) method at the M06-2X/6-31G(d) level, and simulated electronic absorption spectra of these compounds were calculated by the time-dependent (TD) DFT method at the B3LYP/6-31G(d) level of theory. As a result, the lowest energy band was found to consist mainly of a HOMO → LUMO transition. Figure 3 displays the HOMO and LUMO of **3b**. The HOMO was spread over the azahelicene π-plane, whereas the LUMO shows a biased distribution located around the 4-cyanophenyl substituent. This result indicated that the lowest energy band is attributed to a charge-transfer transition from the azahelicene unit to the 4-cyanophenyl substituent. The electrostatic potential map in Figure 3c also indicates the polarized charge distribution of **3b**, suggesting the presence of an ICT. Similar calculational results were obtained for **3c**, **3d**, **5a**, and **5c**, which have electron-withdrawing substituents (Figures S46–S51).
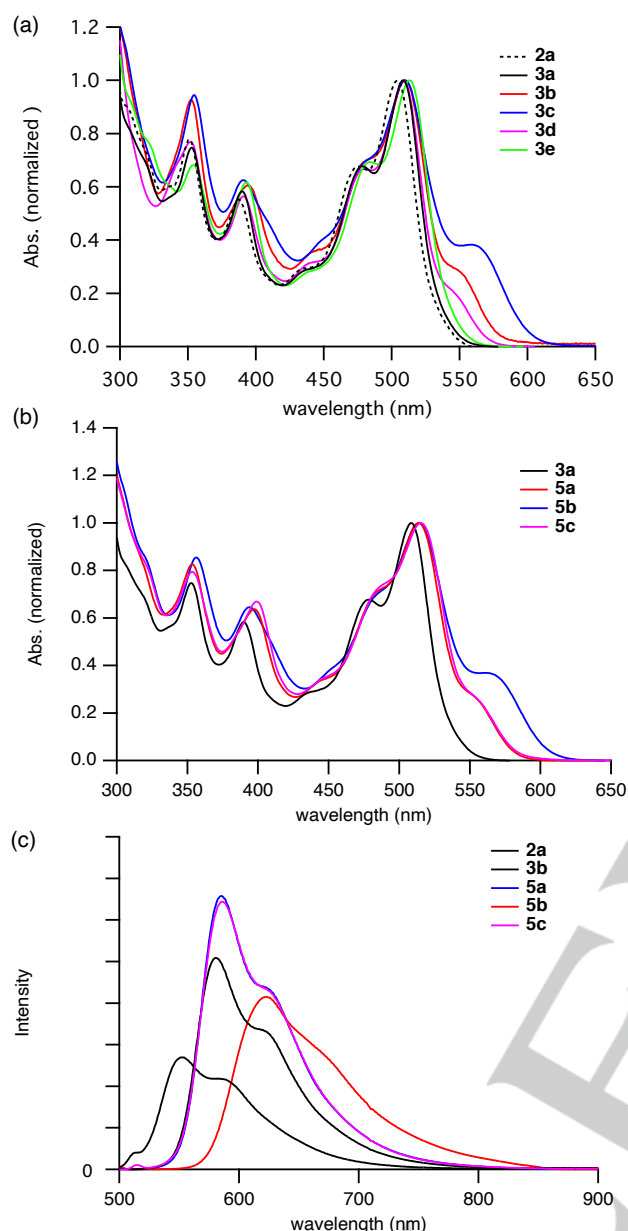
(a) UV/vis absorption spectra

(b) UV/vis absorption spectra

(c) Fluorescence spectra

Figure 2. UV/vis absorption spectra of (a) **2a**, **3a**, **3b**, **3c**, **3d**, and **3e** and of (b) **3a**, **5a**, **5b**, and **5c** in toluene. (c) Fluorescence spectra of **2a**, **3b**, **5a**, **5b**, and **5c** in toluene.
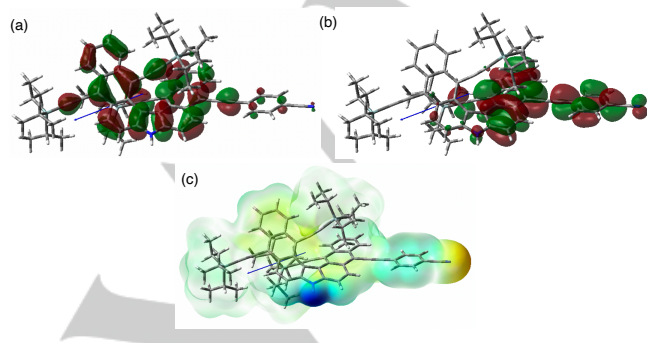

Figure 3. (a) HOMO and (b) LUMO of **3b** calculated by the DFT method (M06-2X/6-31G(d)). (c) Electrostatic potential map of **3b**. The blue arrow represents the vector of the dipole moment of **3b**.

Figure 2c exhibits the fluorescence spectra of **2a**, **3b**, **5a**, **5b**, and **5c** in toluene. The fluorescence quantum yields (Φ_f) were increased upon installing aryl substituents on **2a** (Table S3). In particular, **3b** exhibited the largest quantum yield (Φ_f = 0.66). Similar to the observations in the UV/vis absorption spectra, the emission maxima were shifted to longer wavelengths by installing groups with more electron-withdrawing nature. In the UV/vis absorption spectra, the lowest energy bands of **3b**, **3c**, **3d**, **5a**, and **5b** exhibited solvent-dependent behaviors. The bands shifted to lower energy regions as the solvent polarity increased. The emission spectra also exhibited solvent dependency (Figures S38-S43). The changes were more apparent than those observed for the UV/vis absorption spectra. In addition, the emission efficiency was reduced in polar solvents. From these results, we constructed Lippert-Mataga plots of all compounds, all of which exhibited linear and positive slopes. These results indicate the more polar nature of the excited states compared with the nature of the ground states. In particular, the slopes of the nitro derivatives **3c** and **5b** are steeper than those of the other derivatives, reflecting a greater electron-accepting nature of the nitro group. These analyses confirm the ICT characteristics of these compounds; hence, the presence of dipole moments. Consequently, the ground state dipole moments of **3b**, **3c**, **3d**, **5a**, and **5b** were determined to be 6.03, 6.51, 3.61, 7.34, and 7.79 Debye by theoretical calculations (M06-2X/6-31G(d), Table S4). The directions of the dipole moments for all compounds were from the azahelicene core to the aryl-substituents, which is comparable to the direction of the ICT interactions (Figure 3c).

Figure 4 displays the packing of two molecules each for **2a**, (**M**)-**3b**, and **5a** in the crystal state. In **2a**, two molecules form a π-dimer, in which the NH bonds of each molecule point in opposite directions. The distance between the closest mean planes is 3.35 Å, indicating the presence of π-π stacking interactions. The molecules of (**M**)-**3b** are aligned in a parallel manner to the 1D-chain columnar assembly in the crystal. The 4-cyanophenyl substituent of one molecule is placed directly over the aza[5]helicene unit of the adjacent molecule in a face-to-face fashion. The distance between the mean planes of the two units is 3.51 Å, indicating the presence of π-π stacking interactions. A TIPS group at the internal position of one molecule is also close to the external TIPS substituent of the adjacent molecule. To elucidate the essential factors for 1D-chain columnar orientation in the crystal, we investigated the substituent effect on crystal packing. In **3c** and **3d**, the aryl substituents were placed in parallel over the aza[5]helicene unit of an adjacent molecule, indicating the presence of π-π stacking interactions (Figures S32, S34). The mean plane distance was increased for **3d** to be 3.78 Å, while the distance became shorter for **3c** and (**M**)-**3c** (3.44 Å and 3.45 Å, respectively). Compound **3e** showed a different stacking fashion in the crystal. The 1D columnar orientation has been observed in **3b**. The phenyl substituent was tilted by 23.8° toward the connecting aza[5]helicene unit and formed an intermolecular CH-π interaction rather than a π-π interaction with the adjacent aza[5]helicene-containing molecule (Figure S35). Instead, π-π stacking has been formed with another azahelicene unit in the neighboring column. These facts indicate that the installation of an aryl substituent on one side is essential for the construction of a 1D chain columnar orientation in crystal. However, two molecules of **5a** in the crystal were aligned in an anti-parallel

4

manner to form a π-dimer in the crystal. The 4-cyanophenyl substituent of each molecule is placed over the π-plane of another aza[5]helicene molecule, with a mean plane distance of 3.42 Å. Similar anti-parallel packing was also observed for **5c** (Figure S37). In both cases, the 4-cyanophenyl substituent formed a geometry with a greater degree of coplanarity to the connecting anthracene units than the geometry for **3b** did, indicating the presence of more efficient π-π interactions in molecules with a 4-cyanophenyl substituent than in the other molecules. These facts

indicate that the TIPS substituent at the other side of the aryl substituent is also important to achieving 1D chain columnar orientation. In azahelicene derivatives that form 1D chain columnar structures in the crystal, the TIPS substituent at the external position is placed close to another azahelicene unit in the same column. The closest distance from the mean plane of the anthracene unit is within 3.29 to 3.68 Å, indicating the presence of CH-π interactions.
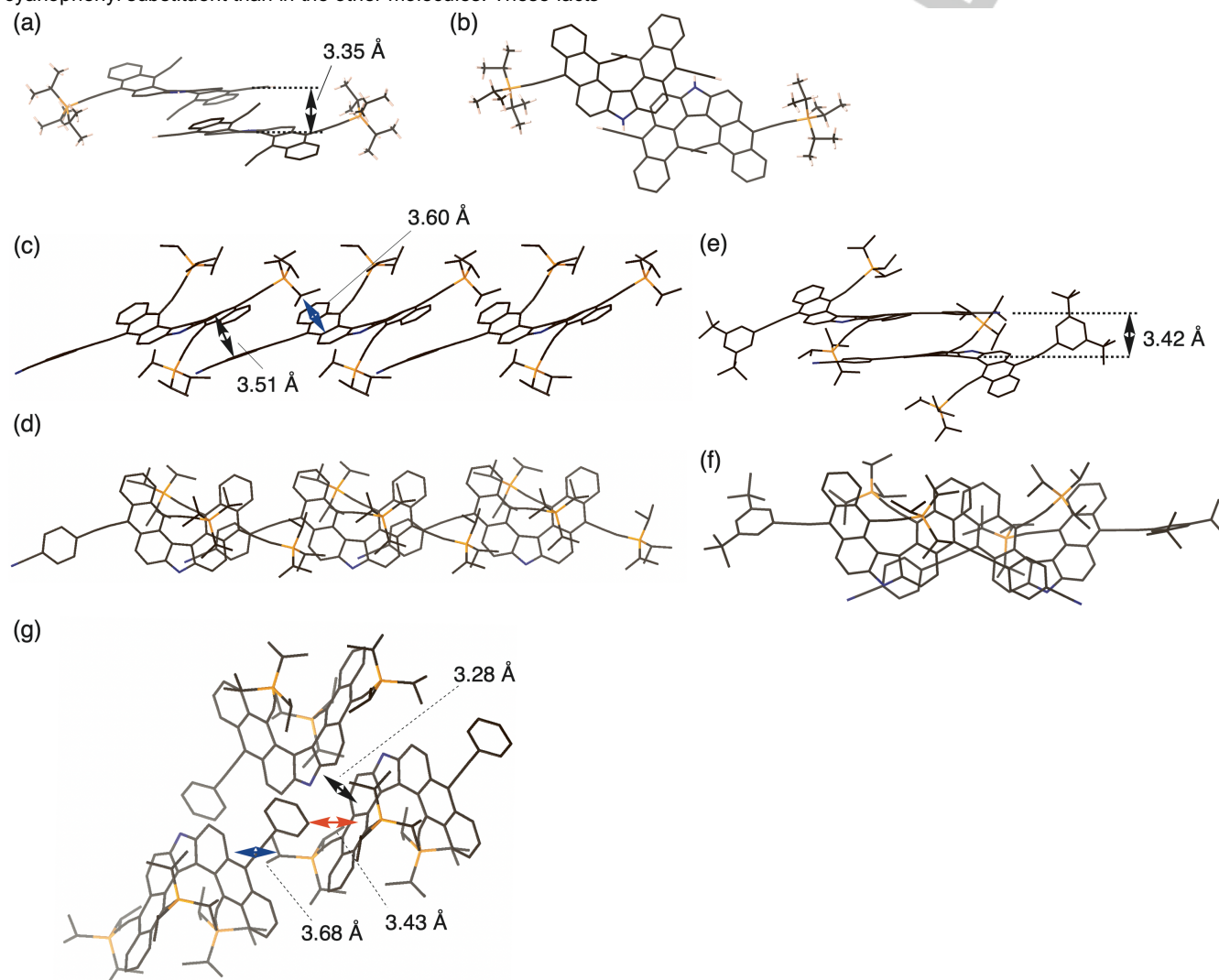

Figure 4. Crystal packing structures of (a) and (b) **2a**, (c) and (d) (**M**)-**3b**, (e) and (f) **5a**, and (g) **3e**. Hydrogen atoms in all figures are omitted for clarity. Black axes represent the distances between two mean planes, and blue and red axes represent the distances between a mean plane and the closest atom.

Looking at the entire structure in the crystal, 1D chain columns of (**M**)-**3b**, **3c**, (**M**)-**3c**, and **3d** were aligned in parallel. In racemic mixtures such as **3c** and **3d**, each 1D chain column is aligned in the opposite direction to the other column, resulting in non-polarity. However, in (**M**)-**3b**, and (**M**)-**3c**, the 1D chain columns are aligned in the same direction, constructing polar crystals (Figure 5). Figure 5c and d displays molecular stacks of neighboring molecules of **3c** and (**M**)-**3c** in different columns, in which a (**P**)-type and a (**M**)-type molecule have constructed a heterodimeric structure. The closest C-C distance between the TIPS group and the adjacent aryl substituent was 3.47 Å, indicating the presence of CH-π interactions. Similar interactions were observed in (**M**)-

3c. In this case, a heterodimeric structure, similar to that observed for **3c,** could not be formed because of steric hindrance.
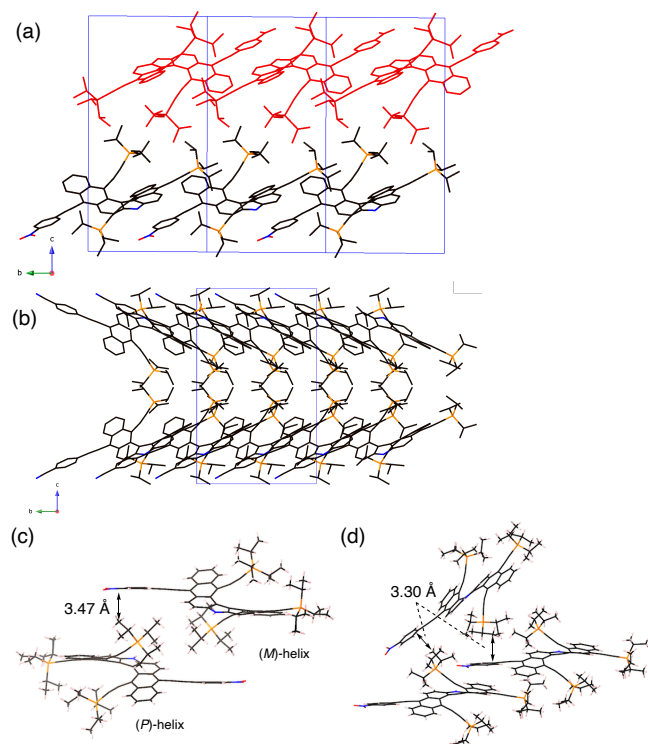
Figure 5. The view of molecular orientations from the *a*-axis for the crystals of (a) **3c** and (b) (*M*)-**3c**. The packing geometries of neighboring dimers in crystal (c) **3c**, and (d) (*M*)-**3c**. The hydrogens and solvent molecules are omitted for clarity. In the crystal packings, the molecules highlighted with red color represent (*P*)-helix enantiomers and the others are (*M*)-helix enantiomers.

Figure 6 exhibits the Hirshfeld surfaces of (*M*)-**3b**. The d_{norm} surface analysis (Figure 6a, and 6b) revealed the presence of π-π interactions between the aryl substituent and the azahelicene unit. Moreover, the d_e surface clearly indicated the presence of intramolecular CH-π interactions between the TIPS substituents and azahelicene units (Figures 6c and 6d). The percentage of surface areas corresponding to intermolecular C–C or C-H contacts for the Hirshfeld surfaces can be a good index for the contribution of π-π or CH-π interactions, respectively. Table S6 summarized these contacts for **3b**, **3c**, **3d**, **3e**, and **5a**. For all compounds, the percentage of C-C contacts is much smaller than that of C-H contacts, indicating that CH-π interactions are dominant for intermolecular interactions. The energy components of the intermolecular interactions of **3c** were further calculated by DFT methods at the CE-B3LYP/6-31G(d) level (Table S7). As a result, the contribution of dispersion energy is remarkable, indicating that both van der Waals interactions between the bulky TIPS substituents and π-π interactions are important for the orientation. The surface of (*M*)-**3b** mapped with d_e shows close contact between the TIPS substituents of the molecule and the aryl substituents of the neighboring azahelicene molecule through CH-π interactions (site B in Figure 6c). Considering the result of the fingerprint analysis, which indicates that the π-π interaction is minor, the dispersion force contributed by the TIPS substituent mainly determines intercolumnar orientation in the crystal. The same orientation was also observed for (*M*)-**3c**. Thus, the presence of a TIPS substituent at both internal and external positions and an electron-withdrawing aryl substituent at the external position are necessary for creating polar crystals with π-extended aza[5]helicenes.
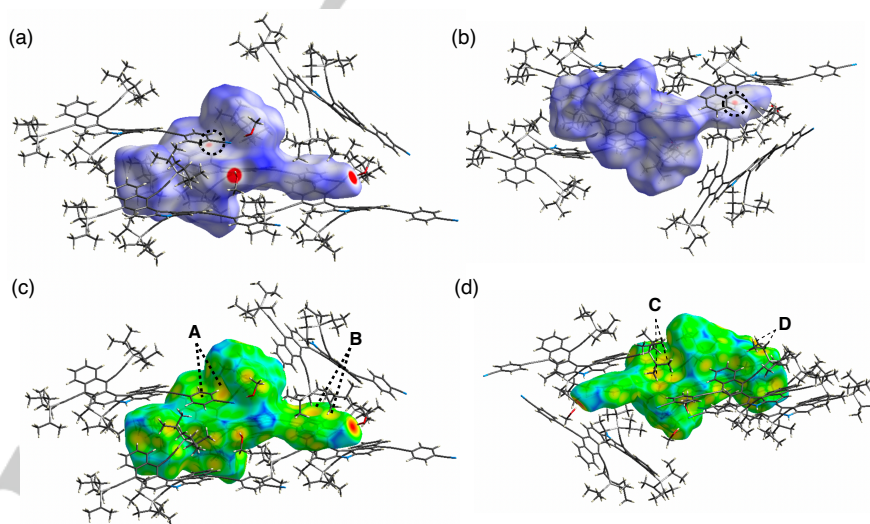

Figure 6. Hirshfeld surfaces of (*M*)-**3b** mapped with (a) and (b) d_{norm} and with (c) and (d) d_e. The red sites highlighted by dotted circles in (a) and (b) represent contacts closer than the sum of van der Waals radii between the aryl substituents and the neighboring azahelicene units. The sites highlighted with the capital letters A–D in (c) and (d) represent the close contacts of CH bonds with the azahelicene unit.

We finally investigated the polarizability of the obtained crystals. Experimental measurements, however, proved to be difficult because of the fragile features of these molecules and because these crystals were too small to connect electrodes directly to them. Therefore, we determined the polarizability of (*M*)-**3b** and (*M*)-**3c** by theoretical calculations. First-principle calculations have often been used for the calculation of the polarizability of organic crystals.[22] We used the Berry phase theory for determining the spontaneous polarizability of these crystals. The results are summarized in Table S8. As shown, the polarizability of (*M*)-**3b** along the b* axis, which is the direction of the molecular dipole moment, was 1.45 μC/cm^{-2}. The value

increased for **(M)-3c** to be 4.53 µC/cm^{-2}, reflecting the more polar nature of **(M)-3c** relative to **(M)-3b** (Figure S55). The polarizabilities along the *c** axis for both **(M)-3b** and **(M)-3c** were much smaller than the polarizabilities of the other molecules, justifying the calculated values. The value of 4.53 µC/cm^{-2} is lower than those for inorganic ferroelectric materials, but comparable to the reported organic ferroelectric compounds.[23] This value certifies the first example of a helicene-based polar crystal.

Conclusion

In summary, we succeeded in the creation of polar assemblies with unsymmetrically substituted aza[5]helicenes prepared through regioselective protiodesilylation reactions. The polar nature of the aza[5]helicenes was characterized by solvent-dependent optical analysis, which established the presence of intramolecular charge-transfer interactions. Crystallographic analysis revealed the presence of three types of molecular packings for aza[5]helicenes. The absence of electron-withdrawing aryl substituents favored the construction of molecules in a face-to-face packing mode, in which each NH group pointed in the opposite direction of its neighbor. Installing electron-withdrawing aryl substituents at the edge of the alkyne group changed the packing directions, so that the NH groups aligned in the same direction. Hirshfeld surface analysis revealed the importance of CH-π interactions for the construction of 1D chain columnar orientation with polar aza[5]helicenes. Furthermore, the CH-π interactions also contributed to intercolumnar orientations. Consequently, TIPS substituents at both internal and external positions of helicenes played a significant role in the crystal packing of aza[5]helicenes. Finally, we determined the polarizability of the present crystals through theoretical calculations. The values are fairly consistent with the ferroelectric organic crystals. These results should enhance helicene chemistry to enable the synthesis of polar organic materials that can be applied to piezo- and pyroelectric materials. Further research into material applications with unsymmetrically substituted aza[5]helicenes is being pursued.

Acknowledgements

[1] a) G. R. Desiraju, *Angew. Chem. Int. Ed.* **2007**, *46*, 8342. b) G. R. Desiraju, *J. Am. Chem. Soc.* **2013**, *135*, 9952. c) C. V. KrishnamohanSharma, *Cryst. Growth Des.* **2002**, *2*, 465. d) Z. Chen, A. Lohr, C. R. Saha-Möllera, F. Würthner, *Chem. Soc. Rev.* **2009**, *38*, 564.

e) Y. Guo, L. Xu, H. Liu, Y. Li, C.-M. Che, Y. Li, *Adv. Mater.* **2015**, 27, 985. f) H. Jiang and W. Hu, *Angew. Chem. Int. Ed.* **2020**, *59*, 1408.

[2] Reviews for polar organic crystals to see: a) S. Horiuchi, Y. Tokura, *Nat. Mater.* **2008**, *7*, 357. b) S. Guerin, S. A. M. Tofail, D. Thompson, *NPG Asia Mater.* **2019**, 11:10. c) T. Vijayakanth, D. J. Liptrot, E. Gazit, R. Boomishankar, C. R. Bowen, *Adv. Funct. Mater.* **2022**, *32*, 2109492.

[3] a) F. Würthner, *Acc. Chem. Res.* **2016**, *49*, 868. b) Q. Miao, M. Lefenfeld, T.-Q. Nguyen, T. Siegrist, C. Kloc, C. Nuckolls, *Adv. Mater.* **2005**, *17*, 407. c) D. Bialas, E. Kirchner, M. I. S. Röhr, F. Würthner, *J. Am. Chem. Soc.* **2021**, *143*, 4500.

[4] a) R. Glaser, *Acc. Chem. Res.* **2007**, *40*, 9. b) E. Meirzadeh, I. Weissbuch, D. Ehre, M. Lahav, I. Lubomirsky, *Acc. Chem. Res.* **2018**, *51*, 1238. b) S. Yagai, S. Okamura, Y. Nakano, M. Yamauchi, K. Kishikawa, T. Karatsu, A. Kitamura, A. Ueno, D. Kuzuhara, H. Yamada, T. Seki, H. Ito, *Nat. Commun.* **2014**, *5*, 4013.

[5] M. A. Petrukhina and L. T. Scott, Fragments of Fullerenes and Carbon Nanotubes: Designed Synthesis, Unusual Reactions, and Coordination Chemistry, Wiley, Hoboken, **2012**.

[6] a) T. Amaya, S. Seki, T. Moriuchi, K. Nakamoto, T. Nakata, H. Sakane, A. Saeki, S. Tagawa, T. Hirao, *J. Am. Chem. Soc.* **2009**, *131*, 408. b) A. Wakamiya, H. Nishimura, T. Fukushima, F. Suzuki, A. Saeki, S. Seki, I. Osaka, T. Sasamori, M. Murata, Y. Murata, H. Kaji, *Angew. Chem. Int. Ed.* **2014**, *53*, 5800.

[7] a) B. M. Schmidt, B. Topolinski, M. Yamada, S. Higashibayashi, M. Shionoya, H. Sakurai, D. Lentz, *Chem. Eur. J.* **2013**, *19*, 13872. b) B. M. Schmidt, B. Topolinski, P. Roesch, D. Lentz, *Chem. Commun.* **2012**, *48*, 6520. c) S. Sanyal, A. K. Manna, S. K. Pati, *ChemPhysChem.* **2014**, *15*, 885.

[8] a) Y. Shoji, T. Kajitani, F. Ishiwari, Q. Ding, H. Sato, H. Anetai, T. Akutagawa, H. Sakurai and T. Fukushima, *Chem. Sci.* **2017**, *8*, 8405. b) Y. Lizumi, Z. Liu, K. Suenaga, S. Okada, S. Higashibayashi, H. Sakurai and T. Okazaki, *ChemNanoMat*, **2018**, *4*, 557.

[9] a) M. A. Majewski and M. Stępień, *Angew. Chem. Int. Ed.* **2019**, *58*, 86. b) K. Miki and K. Ohe, *Chem. Eur. J.* **2020**, *26*, 2529. c) M. Saito, H. Shinokubo and H. Sakurai, *Mater. Chem. Front.* **2018**, *2*, 635. d) W. Wang and X. Shao, *Org. Biomol. Chem.* **2021**, *19*, 101. e) H. Sakurai, *Bull. Chem. Soc. Jpn.* **2021**, *94*, 1579.

[10] a) M. R. Golder and R. Jasti, *Acc. Chem. Res.* **2015**, *48*, 557. b) T. Amaya and T. Hirao, *Chem. Rec.* **2015**, *15*, 310. c) L. T. Scott, *Pure Appl. Chem.* **1999**, *71*, 209. d) M. Jakubec and J. Storch, *J. Org. Chem.* **2020**, *85*, 13415.

[11] a) Y. Shen, C.-F. Chen *Chem. Rev.* **2012**, *112*, 1463. b) M. Gingras *Chem. Soc. Rev.* **2013**, *42*, 968. c) M. Gingras, G. Félix, R. Peresutti *Chem. Soc. Rev.* **2013**, *42*, 1007.

[12] a) F. Pop, N. Zigon, N. Avarvari *Chem. Rev.* **2019**, *119*, 8435. b) N. Saleh, C. Shen, J. Crassous, *Chem. Sci.*, **2014**, *5*, 3680. c) E. S. Gauthier, R. Rodríguez, J. Crassous, *Angew. Chem. Int. Ed.* **2020**, *59*, 22840. d) W.-L. Zhao, M. Li, H.-Y. Lu, C.-F. Chen, *Chem. Commun.*, **2019**, *55*, 13793.

[13] X. Quan, C. W. Marvin, L. Seebald, G. R. Hutchison, *J. Phys. Chem. C* **2013**, *117*, 16783.

[14] O. Stetsovych, P. Mutombo, M. Švec, M. Šámal, J. Nejedlý, I. Císařová, H. Vázquez, M. Moro-Lagares, J. Berger, J. Vacek, I. G. Stará, I. Starý, P. Jelínek, *J. Am. Chem. Soc.* **2018**, *140*, 940.

[15] a) E. Murguly, R. McDonald and N. R. Branda, *Org. Lett.* **2000**, *2*, 3169. b) C. Schaack, A. M. Evans, F. Ng, M. L. Steigerwald and C. Nuckolls, *J. Am. Chem. Soc.* **2022**, *144*, 42. c) F. Zhang, K. Radacki, H. Braunschweig, C. Lambert and P. Ravat, *Angew. Chem. Int. Ed.* **2021**, *60*, 23656. d) H. Anetai, T. Takeda, N. Hoshino, H. Kobayashi, N. Sato, M. Shigeno, M. Yamaguchi and T. Akutagawa, *J. Am. Chem. Soc.* **2019**, *141*, 6. e) Y. Suzuki, N. Tonai, A. Saeki and I. Hisaki, *Chem. Commun.* **2020**, *56*, 13369.

[16] a) T. Hatakeyama, S. Hashimoto, T. Oba, M. Nakamura, *J. Am. Chem. Soc.* **2012**, *134*, 19600. b) K. Nakano, H. Oyama, Y. Nishimura, S. Nakasako, K. Nozaki, *Angew. Chem. Int. Ed.* **2012**, *51*, 695. c) K. Usui, K. Yamamoto, Y. Ueno, K. Igawa, R. Hagihara, T. Masuda, A. Ojida, S. Karasawa, K. Tomooka, G. Hirai, H. Suemune, *Chem. Eur. J.* **2018**, *24*, 14617. d) F. Wang, F. Wang, F. Gan, C. Shen, H. Qiu, *J. Am. Chem. Soc.* **2020**, *142*, 16167.

[17]   C. Zhang, Y. Guo, D. He, J. Komiya, G. Watanabe, T. Ogaki, C. Wang, A. Nihonyanagi, H. Inuzuka, H. Gong, Y. Yi, K. Takimiya, D. Hashizume, D. Miyajima, *Angew. Chem. Int. Ed.* **2021**, *133*, 3298.

[18]   a) K. Goto, R. Yamaguchi, S. Hiroto, H. Ueno, T. Kawai, H. Shinokubo *Angew. Chem. Int. Ed.* **2012**, *51*, 10333. b) A. Ushiyama, S. Hiroto, J. Yuasa, T. Kawai, H. Shinokubo, *Org. Chem. Front.* **2017**, *4*, 664.

[19]   a) A. Ushiyama, H. Shinokubo, S. Hiroto *Chem. Lett.* **2019**, *48*, 1069. b) S. Hiroto *Bull. Chem. Soc. Jpn.* **2020**, *93*, 1334.

[20]   S. Kim, B. Kim, J. In, *Synthesis* **2009**, 1963.

[21]   Crystallographic data for **2a**, (**M**)-**3b**, **3c**, (**M**)-**3c**, **3d**, **3e**, **5a,** and **5c** have been deposited with the Cambridge Crystallographic Data Centre (CCDC) as supplementary publication no. CCDC-2183472, 2183473, 2183474, 2183475, 2183476, 2183477, 2183478, and 2183479.

[22]   a) I. Bprriello, G. Cantele, D. Ninno, G. Iadonisi, *Phys. Rev. B* **2009**, *79*, 125126. b) M. Shepelenko, A. Hirsch, N. Varsano, F. Beghi, L. Addadi, L. Kronik, L. Leiserowitz, *J. Am. Chem. Soc.* **2022**, *144*, 5304.

[23]   F. Ishii, N. Nagaoka, Y. Tokura, K. Terakura, *Phys. Rev. B* **2006**, *73*, 212105.

Entry for the Table of Contents

Insert graphic for Table of Contents here.
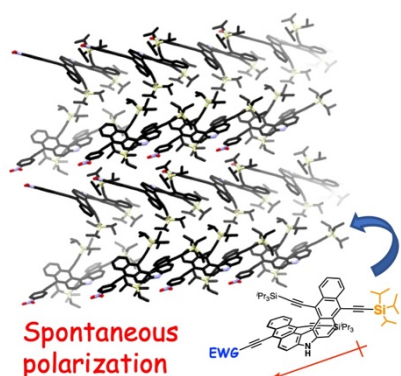
Assembling curved π-conjugated molecules in polar manner have attracted interest for the potential applications to polar materials with piezo- and ferroelectricity. However, strategies for controlling their assembly remain challenging. Here we report examples of polar assemblies with heterohelicenes and reveal the importance of side-chain substituents to spontaneous polarization.